Neonatal insulin action impairs hypothalamic neurocircuit formation in response to maternal high fat feeding

Merly C. Vogt[1,2,4], **Lars Paeger**[3,4], **Simon Hess**[3,4], **Sophie M. Steculorum**[1,2,4], **Motoharu Awazawa**[1,2,4], **Brigitte Hampel**[1,2,4], **Susanne Neupert**[3], **Hayley T. Nicholls**[1,2,4], **Jan Mauer**[1,2,4], **A. Christine Hausen**[1,2,4], **Reinhard Predel**[3], **Peter Kloppenburg**[3,4], **Tamas L. Horvath**[6,#], and **Jens C. Brüning**[1,2,4,5,#]

[1] Max Planck Institute for Neurological Research, D-50931 Cologne, Germany

[2] Department of Mouse Genetics and Metabolism, Institute for Genetics, University of Cologne, D-50674 Cologne, Germany

[3] Biocenter, Institute for Zoology, University of Cologne, D-50674 Cologne, Germany

[4] Excellence Cluster on Cellular Stress Responses in Aging Associated Diseases (CECAD) and Center of Molecular Medicine Cologne (CMMC), University of Cologne, D-50674 Cologne, Germany

[5] Center for Endocrinology, Diabetes and Preventive Medicine (CEDP), University Hospital Cologne, D-50924 Cologne, Germany

[6] Program in Integrative Cell Signaling and Neurobiology of Metabolism, Section of Comparative Medicine, Department of Obstetrics/Gynecology and Reproductive Sciences, Yale University School of Medicine, New Haven, CT, USA

Summary

Maternal metabolic homeostasis exerts long-term effects on the offspring's health outcomes. Here, we demonstrate that maternal high fat diet (HFD)-feeding during lactation predisposes the offspring for obesity and impaired glucose homeostasis in mice, which is associated with an impairment of the hypothalamic melanocortin circuitry. Whereas the number and neuropeptide expression of anorexigenic proopiomelanocortin-(POMC) and orexigenic agoui-related peptide (AgRP)-neurons, electrophysiological properties of POMC-neurons and posttranslational processing of POMC remain unaffected in response to maternal HFD-feeding during lactation, the formation of POMC- and AgRP-projections to hypothalamic target sites is severely impaired. Abrogating insulin action in POMC-neurons of the offspring prevents altered POMC-projections to the preautonomic paraventricular nucleus of the hypothalamus (PVH), pancreatic parasympathetic innervation and impaired glucose-stimulated insulin-secretion in response to maternal overnutrition. These experiments reveal a critical timing, when altered maternal metabolism disrupts metabolic homeostasis in the offspring via impairing neuronal projections and that abnormal insulin signaling contributes to this effect.

#Address correspondence to: Jens C. Brüning, MD bruening@nf.mpg.de Tamas L. Horvath, DVM, PhD tamas.horvath@yale.edu.

Introduction

The sustained global rise in the prevalence of obesity and type 2 diabetes mellitus (T2DM) over the last decades increasingly affects young adults and children (Ludwig and Ebbeling, 2001; Sabin and Shield, 2008). Thus, 15-40 % of pregnancies are complicated by maternal obesity and 3-10 % by maternal diabetes (Anna et al., 2008; Yu et al., 2013). Several human epidemiological studies have demonstrated that maternal obesity, and maternal diabetes and hyperglycemia, even independent of an elevated body mass index or genetic background, predispose the offspring to the development of metabolic disorders (Clausen et al., 2008; Deierlein et al., 2011; Pedersen, 1971). To date, little is known about the cellular and molecular mechanisms underlying this phenomenon known as "metabolic programming". Nonetheless, a broad range of studies has demonstrated that an abnormal hormonal milieu during development triggers persistent changes in the function of hypothalamic neurocircuits, which physiologically regulate energy and glucose metabolism (Plagemann, 2012; Sullivan and Grove, 2010). The hypothalamus integrates hormonal and nutritional signals from the periphery of the organism and conveys them into neuroendocrine and/or autonomic responses (Belgardt and Bruning, 2010; Marino et al., 2011; Vogt and Bruning, 2013). Key players in this neuronal network are the anorexigenic POMC and the orexigenic AgRP/neuropeptide Y (NPY)-coexpressing neurons (Gropp et al., 2005; Luquet et al., 2005). These functionally antagonistic neuronal populations reside in the arcuate nucleus of the hypothalamus (ARH) and mediate their effects via second order neurons mainly located in other key parts of the hypothalamus, such as the PVH, the dorsomedial nucleus of the hypothalamus (DMH) and the lateral hypothalamic area (LH) (Konner et al., 2009).

In contrast to humans, development of these hypothalamic neurocircuits in rodents is not completed at birth, but continues until the third week of postnatal life: Whereas neuronal cell numbers are determined in-utero, formation of functional neuronal networks with the ontogeny of axonal projections and synaptic connections, occurs postnatally during the lactation phase (Bouret et al., 2004a; Grayson et al., 2006; Koutcherov et al., 2003). Importantly, as a result of impaired maternal health, exposure to an altered developmental environment during both of these stages, results in gross changes of these hypothalamic neurocircuits, including differential neuropeptide gene expression, altered hypothalamic neuronal cell numbers, as well as impaired formation of hypothalamic axonal projections (Plagemann, 2012; Sullivan and Grove, 2010). However, differences in study design, in particular in severity, duration and onset of abnormal environmental cues (Kim et al., 2011; Plagemann, 2012) has made it challenging to clearly define i. the exact timing requirements of metabolic insults to affect the metabolic fate of the offspring and ii. the specific molecular mechanisms underlying these persistent cellular changes. Thus, we aimed to establish a mouse model of metabolic programming that would allow us to identify the most sensitive period of hypothalamic neurocircuit development in response to maternal HFD-feeding. Importantly, we further employed this model to delineate the distinct role of neuron-specific insulin signaling in mediating the lifelong predisposition for metabolic disorders in offspring of obese and/or hyperglycemic mothers (Horvath and Bruning, 2006).

Results

Critical timing of maternal high fat feeding on metabolic programming in the offspring

To determine the most vulnerable time frame of hypothalamic neurocircuit development in response to maternal HFD-feeding, we fed female C57Bl/6 virgin mice either a control normal chow diet (NCD) or a HFD for 8 weeks prior to gestation (Figure S1). HFD-feeding for the period of 7 weeks resulted in moderately increased body weight (Figure 1A), elevated fasting blood glucose concentrations (Figure 1B) and an approximately 7-fold-increase in the homeostatic model assessment indices of insulin resistance (HOMA-IR) (Figure 1C), indicating that pre-gestational HFD-feeding causes insulin resistance. During gestation, the mice were maintained on the same diet that they received during the pre-gestational period. At the day of birth (DOB), litter size was adapted to 6-7 pups per mother to assure the same quantitative nutritional availability for each litter, since small litter size increases the propensity for metabolic diseases in the offspring during adulthood (Habbout et al., 2013). At DOB, half of the NCD-fed mothers were exposed to a HFD (i.e. NCD/NCD and NCD/HFD), and half of the mothers fed a HFD pre-gestationally and during gestation were exposed to a NCD during the period of lactation (i.e. HFD/NCD and HFD/HFD). Interestingly, HFD-exposure during lactation, independent of the prenatal maternal diet, resulted in a slight elevation of serum insulin concentrations in the mothers (Figure 1D), and in increased serum insulin levels in the offspring at 3 weeks of age (Figure 1E). After weaning, all offspring were fed a NCD until the age of 8 weeks, after which each group of offspring was divided into groups either exposed to a NCD or a HFD for the following 12 weeks, resulting in a total of 8 different groups of offspring that differed in the prenatal maternal diet, the postnatal maternal diet and in the diet of the offspring after 8 weeks of age (Figure S1).

Maternal HFD-feeding exclusively during lactation predisposes the offspring for metabolic disorders

We first subjected all groups of offspring to a metabolic characterization. When male offspring were fed a NCD, only mice whose mothers were fed a HFD during lactation (NCD/HFD) displayed significantly increased body weight throughout their adult life compared to all other groups (Figure 2A). Consistently, NCD/HFD mice showed elevated body fat content (Figure 2B), increased perigonadal fat pad weight (Figure 2C) and elevated serum leptin levels (Figure 2D) compared to NCD/NCD mice. Moreover, NCD/HFD mice showed enhanced insulin resistance (Figure 2E) and glucose intolerance (Figure 2F) when compared to any other group of offspring. Notably, although most metabolic abnormalities were only seen in male NCD/HFD mice when exposed to a NCD, female offspring from NCD/HFD mothers displayed a similar obese phenotype, only when challenged with a HFD after 8 weeks of age (Figure S2). Taken together, exposure of mothers to a HFD exclusively during the lactation phase exerts the strongest effects on alterations in energy and glucose homeostasis in both male and female offspring.

Effects of maternal HFD-feeding during lactation on hypothalamic neurocircuits

Next, we focused on comparing NCD/NCD and NCD/HFD male offspring to define the molecular mechanism(s) underlying the obese and glucose-intolerant phenotype of

NCD/HFD mice. First, we determined mRNA expression of hypothalamic neuropeptides critically involved in the regulation of energy and glucose homeostasis. Although there was no difference in the expression of ARH neuropeptide genes, i.e. *Pomc, Agrp* and *Npy* (Figure 3A), mRNA expression of one of their anorexigenic downstream targets thyrotropine-releasing hormone (*Trh*), which is predominantly but not exclusively expressed in the PVH (Segerson et al., 1987), was significantly lower in NCD/HFD offspring (Figure 3B). These experiments indicated that in the absence of alterations of *Pomc* and *Agrp*-expression in the ARH, expression of one of the melanocortin-effector pathways is impaired. To determine whether hypothalamic inflammation contributed to the impairment of the melanocortin circuitry, we analyzed mRNA expression of classical inflammatory markers in the hypothalamus. However, we could not detect differences in the hypothalamic expression of any of the genes analyzed between NCD/NCD and NCD/HFD offspring (Figure S3). Next, we analyzed the effect of postnatal maternal HFD-feeding on the cell number of ARH neurons by employing our postnatal feeding paradigm to female C57Bl/6 mice crossed to male transgenic mice expressing the enhanced green fluorescent protein (eGFP) under the transcriptional control of the POMC promoter (POMC[eGFP]) (Cowley et al., 2001); and further to females carrying a floxed Rosa26-tdTomato allele encoding red fluorescent protein (The Jackson Laboratories) crossed to male mice expressing Cre recombinase under the transcriptional control of the AgRP promoter (Tong et al., 2008) to generate AgRP[tdTomato] mice. Consistent with unaltered *Pomc-* and *Agrp/Npy* expression, there was no difference in the number of eGFP-positive POMC, or tdTomato-positive AgRP neurons between NCD/NCD and NCD/HFD offspring (Figure 3C).

Of note, AgRP can be modulated by, but does not depend on posttranslational modifications to decrease TRH expression in the PVH (Creemers et al., 2006; Fekete et al., 2001). However, POMC has to undergo proprotein-convertase (PC)-1, -2 and carboxypeptidase (CPE)-mediated processing to generate the active neuropeptide alpha-melanocyte-stimulating-hormone (α-MSH), which exerts its anorexigenic functions, in part via upregulation of TRH (Fekete et al., 2000). Thus, we investigated whether POMC processing might be impaired in NCD/HFD offspring. Hypothalamic mRNA expression of *Pcsk1, Pcsk 2* (respectively PC-1 and PC-2) and *Cpe* did not show any differences between groups of offspring (Figure 3D). Moreover, MALDI-TOF mass spectrometry of dissected ARH samples showed nearly identical peptide signals, including ions that are mass-identical with products of the POMC precursor protein (i.e. α-MSH, di-acetylated α-MSH and joining peptide) (Pritchard and White, 2007) between NCD/NCD and NCD/HFD offspring (Figure 3E).

Next, we analyzed whether maternal HFD-feeding during lactation had an effect on the electrophysiological properties of POMC neurons in the offspring. Whole-cell and perforated patch clamp recordings on POMC[eGFP] transgenic NCD/NCD and NCD/HFD offspring indicated that maternal HFD-feeding during lactation did not result in any differences in spontaneous firing frequency of POMC-neurons (Figure 3F), POMC-neuron resting membrane potential (Figure 3G), or in the relative synaptic input onto POMC-neurons (Figure 3H). Collectively, these data demonstrate that maternal HFD-feeding exclusively during lactation permanently decreases anorexigenic TRH expression, which is a

target of POMC- and AgRP-neurons of the ARH, without altering ARH neuropeptide gene expression, ARH neuronal cell number, neuropeptide processing of POMC to di-acetylated α-MSH and/or electrophysiological properties of POMC-neurons.

Maternal HFD-feeding exclusively during lactation impairs axonal projections of ARH neurons to intrahypothalamic target sites

Considering that altering maternal diet selectively during lactation, the phase of hypothalamic neurocircuit development in which axonal projections are formed in rodents, had the strongest impact on the metabolic fate of the offspring, we next analyzed the immunoreactivity of α-MSH- and AgRP-containing fibers in three of the main ARH downstream hypothalamic projection areas: the PVH, DMH and LH. Of note, the PVH consists of distinct functional subcompartments that regulate neuroendocrine, behavioral and autonomic responses to control energy and glucose homeostasis (Biag et al., 2012). Neuroendocrine neurons, such as TRH neurons, reside mainly in the anterior two thirds of the PVH (referred to as PVH_{ant}), whereas preautonomic neurons are predominantly found in the posterior part of the PVH (referred to as PVH_{post}) (Biag et al., 2012). Due to this distinct compartmentalization and the associated diverse functions of the PVH, we differentiated both, the PVH_{ant} and the PVH_{post}, in our analysis. Quantification of the fiber density in the PVH_{ant} (Figure 4A), the PVH_{post} (Figure 4B), the DMH (Figure 4C) and the LH (Figure 4D) revealed robust reductions in both, the α-MSH and AgRP fiber densities in NCD/HFD offspring compared to NCD/NCD offspring. Thus, maternal HFD-feeding results in a consistent decrease of ARH neuronal fiber densities in hypothalamic areas critically involved in the neuroendocrine and autonomic regulation of energy homeostasis, likely due to impaired axon formation in the offspring.

Deciphering the role of neuronal insulin signaling in the predisposition for metabolic disorders in NCD/HFD offspring

Although maternal HFD-feeding during lactation did not affect body weight, it significantly increased the glucose and insulin content of the milk in NCD/HFD mothers (Figure S4), which was associated with a distinct hyperinsulinemia in the NCD/HFD offspring at 3 weeks of age (Figure 1E). Thus, we aimed to define the potential contribution of neuronal insulin signaling in impairing melanocortin projections in offspring of postnatally HFD-fed mothers. To this end, we specifically inactivated the insulin receptor (IR) from POMC neurons in NCD/NCD and NCD/HFD offspring by crossing female IR floxed/floxed ($IR^{fl/fl}$) mice with male $IR^{fl/fl}$ mice expressing Cre recombinase under the control of the POMC promoter (Balthasar et al., 2004; Bruning et al., 1998; Konner et al., 2007) and further subjected the mothers to our postnatal feeding paradigm. All groups of offspring were challenged with a HFD after 8 weeks of age, resulting in 4 groups of offspring differing in both, the maternal diet during lactation and in the presence (NCD/NCD ctrl and NCD/HFD ctrl) and absence (NCD/NCD POMC ^{IR} and NCD/HFD POMC ^{IR}) of IR-expression on POMC neurons. Similar to our previous results, maternal HFD-feeding exclusively during lactation did not alter body weight between NCD/NCD ctrl and NCD/HFD ctrl offspring on HFD, and also had no effect on the respective POMC-specific IR-deficient offspring (Figure 5A). Despite showing no increases in body weight, NCD/HFD offspring developed greater adiposity independent of their genotype, as revealed by elevated body fat content (Figure

5B), increased perigonadal fat pad weight (Figure 5C) and elevated serum leptin levels (Figure 5D). Similarly, both measures of insulin sensitivity, i.e. the HOMA-IR (Figure 5E) and insulin tolerance tests (ITT) (Figure 5F) showed tendencies towards an impaired insulin sensitivity in both NCD/HFD ctrl and in NCD/HFD POMC^{IR} offspring. Thus, POMC-specific inactivation of IR-signaling did not affect adiposity, nor the impaired insulin sensitivity in offspring from mothers fed a HFD exclusively during lactation.

However, when subjected to a glucose tolerance test (GTT), NCD/HFD ctrl mice displayed a pronounced glucose intolerance, which was rescued to NCD/NCD levels in NCD/HFD POMC^{IR} offspring (Figure 5G). Together, these results point to a distinct role for elevated neuronal insulin signaling in response to maternal postnatal HFD-feeding in predisposing the offspring for an impaired glucose tolerance throughout lifetime.

POMC-specific IR-deficiency in NCD/HFD offspring prevents altered axonal projections of POMC neurons to preautonomic PVH

To decipher persistent hypothalamic cellular changes responsible for the metabolic rescue of glucose tolerance in NCD/HFD POMC^{IR} mice, we analyzed fiber densities of ARH neurons to the distinct subcompartments of the PVH at 8 and 20 weeks of age, as well as to the DMH and LH at 20 weeks of age. Loss of the IR specifically on POMC neurons did not change α-MSH or AgRP fiber densities to any hypothalamic target site in NCD/NCD offspring at any age (Figure 6A and 6B, Figure S5A and S5B). Moreover, maternal HFD-feeding exclusively during lactation resulted in a decrease of α-MSH fiber density in the neuroendocrine PVH$_{ant}$ in young and old NCD/HFD animals (Figure 6A), as well as in the DMH (Figure S5A) and LH (Figure S5B), independent of their genotype. However, although NCD/HFD POMC^{IR} mice displayed a similar decrease in α-MSH fiber density in the neuroendocrine PVH$_{ant}$ region as their control litter mates (Figure 6A), specific inactivation of the IR on POMC neurons protected against a decrease in the α-MSH fiber density in the preautonomic PVH$_{post}$ compartment resulting in a persistent restoration of α-MSH fiber density in NCD/HFD POMC^{IR} offspring close to NCD/NCD levels both at 8 and 20 weeks of age (Figure 6B).

In contrast, AgRP fiber densities were significantly reduced in NCD/HFD offspring independent of their genotype in the PVH$_{ant}$, DMH, LH and most importantly, also the PVH$_{post}$ at the age of 20 weeks (Figure 6A, 6B, Figure S5A and S5B). Collectively, hyperinsulinemia in response to maternal HFD-feeding during lactation impairs the axonal outgrowth of POMC neurons specifically to the preautonomic compartment of the PVH.

Effects of maternal HFD-feeding during lactation and POMC-specific IR-deficiency on pancreatic β-cells

Reciprocal neural connections between the hypothalamus and preganglionic motor neurons of the autonomic nervous system play an important role in the regulation of energy and glucose homeostasis (Marino et al., 2011). Therefore, we aimed to identify changes in the autonomic tone in peripheral organs that could possibly be linked to the specific restoration of α-MSH axonal projections to the preautonomic compartment of the PVH$_{post}$ in NCD/HFD POMC^{IR} mice. Given the distinct rescue of glucose tolerance in POMC-

specific IR-deficient NCD/HFD offspring in the absence of alterations in insulin sensitivity, we analyzed the parasympathetic innervation of pancreatic β-cells by staining for vesicular acetylcholine transporter (vAChT) (Rossi et al., 2005). Strikingly, the number of vAChT-immunoreactive buttons per islet area was significantly reduced in NCD/HFD ctrl offspring, but rescued to NCD/NCD levels in NCD/HFD POMC [IR] mice (Figure 7A). In line with the decreased parasympathetic innervation of pancreatic β-cells in NCD/HFD ctrl mice, glucose-stimulated insulin-secretion was significantly decreased compared to NCD/HFD POMC [IR] offspring (Figure 7B). Consistently, C-peptide levels were decreased 5 minutes after intravenous glucose injection in NCD/HFD ctrl offspring (Figure 7C). In contrast, this defect in insulin secretion in NCD/HFD ctrl mice was not seen upon L-arginine stimulation (Figure 7D) and was not associated with glucose-stimulated alterations in levels of free fatty acids (FFA) or glucagon-like peptide 1 (GLP-1) (Figure S6). Moreover, neither maternal HFD-feeding during lactation, nor POMC-specific IR-deficiency had any effect on the average pancreatic β-cell-mass or the average islet size of the pancreas (Figure 7E). Taken together, our results indicate that POMC-specific IR-deficiency improves glucose-stimulated insulin secretion presumably in part via modulation of the parasympathetic tone in offspring from postnatally HFD-fed mothers.

Discussion

Heavy mothers have heavy babies – is one oversimplified conclusion from studies demonstrating that maternal obesity, diabetes and hyperglycemia during pregnancy and lactation have long-term effects on the offspring's future health prognoses (Plagemann, 2012; Sullivan and Grove, 2010). To shed more light on the molecular processes underlying this phenomenon also referred to as "metabolic programming", we sought to identify the period(s) of hypothalamic neurocircuit development most strongly perturbed by maternal HFD-feeding to impair energy and glucose homeostasis in the offspring. Our study not only shows that the lactation period in rodents is most sensitive to the altered developmental environment in response to maternal HFD-feeding, predisposing the offspring for metabolic diseases as described before (Sun et al., 2012); but importantly demonstrates that the short exposure to HFD during this distinct developmental phase is sufficient to predispose the offspring for metabolic disorders at least in part via impairing ARH neuronal innervation of intrahypothalamic target areas. This finding is supported by other models of postnatal overnutrition, such as litter size adaptation and cross-fostering experiments demonstrating that an altered milieu during early postnatal environment in rodents is not only sufficient to predispose for metabolic disorders, but can partly override prenatal factors and genetic predisposition to develop obesity (Chen et al., 2008; Glavas et al., 2010; Gorski et al., 2006). Importantly, the sustained impairment of melanocortin projections throughout lifetime in the offspring from mothers exposed to HFD-feeding during lactation clearly highlights the apparent lack of plasticity of the CNS during adulthood to compensate for this developmental defect.

A distinct role for perinatal hyperinsulinemia in mediating metabolic programming in offspring of malnourished or diabetic mothers has been proposed as early as the 1970s (Pedersen, 1971). Since then, several human epidemiological and animal studies have further substantiated this hypothesis, however, without providing direct mechanistic

evidence on how abnormal insulin signaling contributes to the predisposition for metabolic diseases later in life (Harder et al., 1999; Plagemann et al., 1999; Plagemann et al., 1992; Steculorum and Bouret, 2011; Steculorum et al., 2013). Thus, to decipher the relative contribution of neuron-specific insulin signaling in mediating metabolic programming, we genetically ablated the insulin receptor (IR) from POMC-neurons in offspring from postnatally HFD-fed mothers (POMC ^{IR}). In contrast to mice lacking the IR specifically on AgRP-neurons, which display impaired regulation of hepatic glucose production, POMC ^{IR} mice do not have a baseline phenotype (Konner et al., 2007). Thus, employing our feeding paradigm to POMC ^{IR} offspring largely facilitated the interpretation of results and conclusions that could be drawn - as a proof of principle - for the role of hypothalamic insulin signaling during development under pathological conditions. Although insulin had been reported to have axonotrophic effects *in vitro* (Schechter et al., 1999; Toran-Allerand et al., 1988), we did not observe significant differences in POMC axonal formation between ctrl and POMC ^{IR} offspring from NCD-fed mothers suggesting that IR-signaling is not essential for POMC axonal organization under normal developmental conditions. Similarly, we have recently demonstrated that in adult mice, only under obese conditions, activation of insulin signaling in the ventromedial nucleus of the hypothalamus contributes to the diet-induced inhibition of POMC neurons (Klockener et al., 2011). Moreover, offspring from obese mothers in rodents and humans display altered insulin sensitivity, including in the CNS (Catalano et al., 2009; Chen et al., 2008; Gupta et al., 2009; Morris and Chen, 2009). Accordingly, it is conceivable that in our model, neonatal hyperinsulinemia in the offspring could result in an abnormal activation of insulin signaling in POMC neurons, thereby contributing to the disruption of melanocortin projections.

The site-specificity in the rescue of POMC axonal formation to the preautonomic compartment, but not to the neuroendocrine compartment of the PVH in POMC-specific IR-deficient offspring from postnatally HFD-fed mothers, might result from the cellular heterogeneity of this neuronal population. Only a subset of POMC neurons is insulin-responsive and this subpopulation of neurons is distinct from leptin-responsive POMC neurons in the ARH (Williams et al., 2010). Thus, loss of IR-signaling under hyperinsulinemic conditions might only lead to a beneficial effect on a subpopulation of POMC neurons, which might predominantly target the posterior part of the PVH. However, future studies will clearly have to address the mechanistic basis for the selective effect of IR-signaling on projection formation to the PVH. Of note, Bouyer and Simerly have recently demonstrated a similar role for leptin in mediating site-specific axonal innervation of AgRP neurons to the preautonomic compartment of the PVH (Bouyer and Simerly, 2013). However, whether abnormal levels of insulin have identical effects on the axonal projections of AgRP neurons as we described for POMC neurons still requires further investigation.

Although we could show that POMC-specific inactivation of the IR rescues POMC axonal innervation of the preautonomic PVH, as well as glucose tolerance and improves glucose-stimulated insulin secretion in offspring from postnatally HFD-fed mothers, loss of insulin signaling in POMC neurons did neither ameliorate POMC axonal innervation of the neuroendocrine compartment of the PVH, the DMH or LH, nor reduce the susceptibility to develop increased adiposity and insulin resistance. Thus, other mechanisms than abnormal

insulin signaling in POMC neurons must play an important role in mediating metabolic programming in offspring from postnatally HFD-fed mothers. Indeed, maternal HFD-feeding during lactation does not only lead to increased levels of glucose and insulin, but also to elevated levels of leptin and free fatty acids in the milk (Figure S4), presumably contributing to the strong metabolic impairments in offspring exposed to maternal HFD-feeding during lactation. Accordingly, the crucial role of well-balanced leptin levels during hypothalamic neurocircuit development has been established in a series of outstanding studies (Bouret et al., 2004b; Bouyer and Simerly, 2013; Vickers et al., 2005). Apart from leptin, abnormal levels of other hormones such as ghrelin, corticosterone, serotonin or elevated levels of free fatty acids in response to postnatal maternal HFD-feeding might affect hypothalamic neurocircuit development and/or alter cellular plasticity in peripheral organs thereby contributing to the predisposition of metabolic diseases (Bonnin and Levitt, 2011; Grove and Cowley, 2005; Sasaki et al., 2013). Nevertheless, among all the developmental factors that may act synergistically and antagonistically to shape neuronal circuitries, the present study highlights a critical role of insulin in impairing long-term organization of melanocortin projections within the hypothalamus under pathological conditions during development.

Obesity has previously been associated with disturbed functions of the autonomic nervous system (Baum et al., 2013; Greenfield and Campbell, 2008). Consistently, our study suggests that maternal HFD-feeding only during lactation results in reduced pancreatic vagus nerve activity in the offspring. Similarly, offspring from undernourished mothers, which share several metabolic impairments with offspring from obese mothers, were reported to have a decreased pancreatic parasympathetic activity (Gravena et al., 2007). Moreover, perinatal HFD-exposure was shown to reduce hepatic sympathetic innervation in non-human primates (Grant et al., 2012). Thus, altering maternal metabolism during development may further (directly or indirectly) affect downstream autonomic pathways, thereby potentially deteriorating proper regulation of energy and glucose homeostasis in the offspring. Accordingly, POMC- and AgRP-neurons do not only project to intra-hypothalamic areas, but also sparsely innervate distinct regions throughout the CNS, including autonomic control sites in the brainstem and spinal cord (Broberger and Hokfelt, 2001; King and Hentges, 2011), where they act on melanocortin 4 receptors to regulate energy and glucose homeostasis (Rossi et al., 2011; Sohn et al., 2013). Thus, maternal HFD-feeding during lactation and the associated developmental hyperinsulinemia could also affect melanocortin projections to these autonomic control sites directly, thereby contributing to the obese and glucose intolerant phenotype seen in NCD/HFD offspring, a possibility, which clearly deserves further investigation.

Importantly, the establishment of ARH neuronal projections as it occurs during lactation in rodents, occurs predominantly during the third trimester of human pregnancy *in utero* (Grayson et al., 2006; Grove et al., 2005; Koutcherov et al., 2003). Thus, although based on these developmental differences a direct transfer of our results to the human situation warrants caution, our experiments clearly indicate that acute changes in maternal glucose metabolism during this critical time window, i.e. third trimester, may exert detrimental effects on the offspring's health throughout life. Since maternal glucose can freely permeate

the placenta, blood glucose excursions can stimulate insulin secretion in the offspring. In fact, children of mothers with altered glucose metabolism during the last trimester of pregnancy exhibit significant hyperinsulinemia at birth (Metzger et al., 2008). In light of our results, this hyperinsulinemia specifically during the period in which melanocortin-projections are formed, may therefore contribute to the long-term impairment of hypothalamic regulation of energy and glucose homeostasis. Given that gestational diabetes frequently manifests during exactly this critical period (third trimester), our results point towards the necessity of highly-sensitive glucose tolerance screenings and well-controlled anti-diabetic therapy for mothers particularly during this distinct phase of pregnancy independent of their body mass index (Mumtaz, 2000).

Experimental procedures

Animal care

All animal procedures were conducted in compliance with protocols approved by local government authorities (Bezirksregierung Köln) and the Institutional Animal care and Use Committee from Yale University and were in accordance with National Institutes of Health guidelines. Unless otherwise stated, animals were allowed *ad libitum* access to either normal chow diet (#T.2018.R12, Harlan Teklad Global Rodent) containing 53.5 % carbohydrates, 18.5 % protein and 5.5 % fat (12 % fat calories from fat) or high-fat diet (#C1057, Altromin) containing 32.7 % carbohydrates, 20% protein and 35.5 % fat (55.2 % calories from fat) and drinking water. For detailed information regarding maternal diet manipulations, analytical time-points of the offspring, determination of body composition and HOMA-IR, serum analyses and glucose and insulin tolerance tests, see supplementary section.

Glucose- and L-arginine-stimulated insulin secretion

15-week-old, 16-hours-fasted animals were intravenously (i.v.) or intraperitoneally (i.p.) injected with 1 mg g^{-1} body weight of glucose (20 % glucose, Delta Select) or 3 mg g^{-1} body weight L-arginine (Sigma-Aldrich), respectively. Blood samples were collected 0, 2, 5, 15 and 30 minutes after injection. For analysis of glucose-stimulated C-peptide, GLP-1 and FFA levels, blood samples were collected before and 5 minutes after i.v. glucose injection. Samples used for determination of GLP-1 concentration were treated with dipeptidyl peptidase 4 inhibitor (Merck Millipore). For information regarding serum analyses, see supplementary section.

ARH neuronal cell count

For determination of ARH neuronal cell number, POMC and AgRP neurons were counted in NCD/NCD and NCD/HFD POMC[eGFP] and AgRP[tdTomato] offspring, respectively. For detailed information, see supplementary section.

Tissue collection and MALDI-TOF mass spectrometry

The ARH of 20-week-old animals were carefully microdissected under visual guidance using a binocular microscope, then further processed to be subjected to MALDI-TOF mass spectrometry. Mass spectra were manually acquired in positive ion and reflectron mode on an ultrafleXtreme MALDI TOF/TOF mass spectrometer (Bruker Daltonics). ClinPro Tools

software 3.0 (Bruker) was used for comparison of signal intensities of *Pomc*-products; the results are presented as gel view in logarithmic gray scale display mode. For detailed information, see supplementary section.

Electrophysiology

POMC neurons were recorded from NCD/NCD and NCD/HFD POMC[eGFP] transgenic mice (Cowley et al., 2001) at room temperature under current- and voltage-clamp in the perforated patch and whole-cell patch-clamp configuration using an EPC10 patch-clamp amplifier (HEKA). For detailed information, see supplementary section

AgRP and α-MSH immunostaining and analyses

For the analysis of α-MSH and AgRP fiber densities, 8 and 20 week-old male mice were anesthetized and transcardially perfused with phosphate buffered saline (PBS), pH 7.5, followed by 4 % paraformaldehyde (PFA) in borate buffer, pH 9.5 and post-fixed for 4 h in 20 % sucrose 4 % PFA in borate buffer and transferred to 20 % sucrose in PBS overnight. 25 μm-thick sections throughout the hypothalamus were processed for immunofluorescence as previously described (Bouret et al., 2004b; Bouret et al., 2008; Steculorum and Bouret, 2011). Briefly, sections were incubated in goat anti-AgRP (1:4000; Phoenix Pharmaceuticals) or sheep anti-α-MSH (1:40000, Millipore). Secondary Alexa Fluor 488 goat antirabbit IgG or Alexa Fluor 568 donkey anti-sheep IgG (1:200, Life Technologies™) were used to detect primary antibodies. For detailed information regarding picture acquisition and quantification, see supplementary section.

Statistical analyses

Data sets with only two independent groups were analyzed for statistical significance using unpaired two-tailed Student's t-test. Data sets with more than two groups were analyzed using one-way analysis of variance (ANOVA) followed by Tukey's posthoc test. For statistical analyses of body weight gain, the area-under-the-curve (AUC) from week 2 to week 20 was calculated for each mouse and used for further statistical analyses. For statistical analyses of GTTs and ITTs, we performed two-way ANOVAs followed by Bonferroni's posthoc test. Statistically significant outliers were calculated using Grubb's test for outliers. All p-values below 0.05 were considered significant. All displayed values are presented as mean ± SEM; $*p < 0.05$. $**p < 0.01$. $***p < 0.001$ versus all other groups within the same diet after week 8, if not indicated otherwise.

Experimental Procedures

Analysis of body composition

Nuclear magnetic resonance was employed to determine whole-body composition of 20 week-old live animals using the NMR Analyzer minispeq mq7.5 (Bruker Optik, Germany).

Serum analyses

Blood glucose levels were determined from whole venous tail blood using an automatic glucose monitor (GlucoMen Glycó, A.Menarini Diagnostics). Serum insulin, leptin, C-

peptide and GLP-1 levels were measured by enzyme-linked immunosorbent assays according to the manufacturer's instructions (Mouse/Rat Insulin ELISA, Mouse Leptin ELISA, Crystal Chem Inc.; Mouse C-peptide (Mouse) ELISA Kit, ALPCO; GLP-1 ELISA kit, MyBioSource). Serum non-esterified free fatty acids (NEFA) were quantified according to the manufacturer's instructions (WAKO Chemicals GmbH).

Determination of HOMA-IR

The HOMA-IR was calculated as follows: fasting serum insulin concentration (μU/ml) multiplied by fasting blood glucose levels (mg/dl) divided by 405 (Matthews et al., 1985).

Insulin- and Glucose-Tolerance Tests

Insulin-tolerance tests were performed with 14-wk-old animals fed *ad libitum*. After measuring basal blood glucose levels, each animal was intraperitoneally (i.p.) injected with 0.75 U kg^{-1} body weight of insulin (Actrapid; Novo Nordisk A/S). Blood glucose levels were recorded 15, 30 and 60 minutes after injection. Glucose-tolerance tests were carried out on 15-wk-old mice after a 16 h overnight fast. After determination of fasted blood glucose levels, animals were injected i.p. with a bolus of 2 mg mg^{-1} body weight of glucose (20% glucose, Delta Select) and blood glucose levels were monitored 15, 30, 60 and 120 minutes after injection.

Determination of milk composition

At P19, lactating mothers were separated from their pups for 16 h overnight. Milk was manually collected from deeply anesthetized females for a total of 5 minutes and stored at −20°C until further use. Milk insulin and leptin levels were determined by ELISA assays according to the manufacturer's instructions for serum analysis (Mouse/Rat Insulin ELISA, Mouse Leptin ELISA, Crystal Chem Inc, USA). Non-esterified free fatty acids (NEFA) in the milk were quantified according to the manufacturer's instructions for serum analysis (WAKO Chemicals GmbH, Germany). Milk glucose levels were determined using the B-Glucose Analyzer (Hemocue, Germany).

Animal care, maternal diet manipulation and analytical time-points of their offspring

All animals were housed in 3-4 animals per cage at 22-24°C on a 12h light/dark cycle with lights on at 6 am. 3 week-old female C57Bl/6 mice were either fed a NCD or a HFD up to the age of 11 weeks. At the age of 10 weeks, blood glucose levels were determined and whole venous tail blood was collected, after a 16 h overnight fast, to determine fasted serum insulin. Breedings with male C57Bl/6 mice were set up at 11 weeks of age. NCD-fed females were only used for breedings if their HOMA-IR was below or equal to the mean of all NCD-fed females and HFD-fed females were only used for breedings if their HOMA-IR was above this threshold. During gestation, mice were maintained on the same diet they had received before. During lactation, half of the mothers received the other respective diet. At the day of weaning, whole venous tail blood was collected both from the mothers, as well as from their offspring at random fed state. Blood samples were collected from the offspring in the same manner at 8 weeks of age, and, after a 16 h fast, at 15 wks of age before being subjected to a GTT. Body weight of the offspring was measured in the second and third

week of postnatal life, as well as after week 8 on a weekly basis. Offspring for phenotypical analyses were sacrificed in a random-fed state at 20 weeks of age. Every experimental group consists of offspring from at least three different litters. IR$^{fl/fl}$ mothers and their offspring were treated the same way except that they were only fed a NCD prior to and during gestation.

Generation of POMC^{eGFP}, AgRP^{tdTomato} and POMC ^{IR} mice

Mice expressing the POMC^{eGFP} transgene were generated by crossing C57Bl/6 female to transgenic POMC^{eGFP} male mice (Cowley, 2001). To generate AgRP^{tdTomato} offspring, female reporter mice homozygously carrying the B6;129S6-Gt(ROSA)26Sor$^{tm9(CAG-tdTomato)Hze}$/J (The Jackson Laboratories) allele were crossed to AgRPCre$^{pos/neg}$ male mice (Tong et al., 2008). To generate POMC ^{IR} mice, IR$^{fl/fl}$ female mice were mated with POMCCre$^{pos/neg}$, IR$^{fl/fl}$ male mice (Konner et al., 2007). All animals were backcrossed to C57Bl/6J mice for at least 10 generations.

POMC^{eGFP} and AgRP^{tdTomato} neuronal cell count

8-week-old POMC^{eGFP} and AgRP^{tdTomato} mice were transcardially perfused with phosphate buffered saline (PBS), pH 7.5, followed by 4 % paraformaldehyde in PBS, pH 7.5. Brains were dissected, postfixed for 4 h at 4°C in PBS containing 4% PFA and 20% Sucrose, pH 7.5 and cryoprotected overnight in PBS containing 20% Sucrose, pH 7.5. To determine neuronal cell number, 25 μm-thick free-floating coronal sections through the ARH were cut using a cryostat (Leica) and used for the respective staining. eGFP-positive neurons were detected using rabbit anti-GFP antiserum (1:10000, Molecular Probes/Invitrogen). Incubation with secondary Biotin-labeled donkey antirabbit IgG (1:500, Jackson ImmunoResearch) was followed by incubation with the VECTASTAIN Elite ABC kit (Vector Laboratories) and 0.4 % DAB/0.01 % H_2O_2 for 1 h. Pictures were acquired using a Leica DM1000 LED microscope (Leica) equipped with a 10x objective. Pictures of red fluorescent protein in AgRP neurons of AgRP^{tdTomato} offspring were acquired using a confocal Leica TCS SP-8-X microscope (Leica) equipped with a 20x objective. For each animal, neurons were manually counted to obtain the total POMC^{eGFP} and/or AgRP^{tdTomato} neuronal number.

Analysis of gene expression

Hypothalami were dissected using Brain Matrices (Braintree Scientific, Inc.). Isolated mRNA from this tissue was analyzed using quantitative real-time PCR. RNA was isolated using the Qiagen RNeasy Kit (Qiagen), which was combined with the RNase-Free DNase Set (Qiagen). RNA was reversely transcribed with High Capacity cDNA RT Kit and amplified using TaqMan® Universal PCR-Master Mix, NO AmpErase UNG with TaqMan® Assay-on-demand kits (Applied Biosystems). Relative expression of target mRNAs was adjusted for total RNA content by *hypoxanthine guanine phosphoribosyl transferase 1* (*Hprt1*) RNA quantitative PCR. Calculations were performed by a comparative method ($2^{-\Delta\Delta CT}$). Quantitative PCR was performed on an ABI-PRISM 7900 HT Sequence Detection system (Applied Biosystems).

Tissue collection and MALDI-TOF mass spectrometry

The ARH were carefully microdissected under visual guidance using a binocular microscope, then rinsed in distilled water for a few seconds and transferred with a glass capillary into 20 μl methanol/water (1/1) in 1 % formic acid. Dissected tissues were homogenized, sonicated and subsequently centrifuged for 15 min at 13.000 U/min. All steps were performed at 4°C; 0.3μl of the supernatant was pipetted on a stainless steel sample plate for MALDI-TOF mass spectrometry. Remaining supernatants were each filled with 40 μl 0.5 % acetic acid and then evaporated to about 10 μl to reduce the methanol concentration. Samples were refilled, again with 40 μl 0.5 % acetic acid, and loaded onto activated and equilibrated home-made Stage Tips (Rappsilber et al., 2007) filled with C18 discs from Empore™ filter material (Bioanalytical Technologies). After rinsing with 20 μl 0.5 % acetic acid, peptides were eluted using 4 μl of 10/20/25/30/40/50 % acetonitrile in 0.5 % acetic acid, respectively. Each eluate was divided in six portions and applied onto the sample plate for MALDI-TOF mass spectrometry. Dried samples were covered with a mixture of 0.5 μl α-cyano-4-hydroxycinnamic acid (CHCA, Sigma-Aldrich, Germany) dissolved in 50% methanol/water. After drying at room temperature, each spot was finally rinsed with water for a few seconds. Mass spectra were manually acquired in positive ion and reflectron mode on an ultrafleXtreme MALDI TOF/TOF mass spectrometer (Bruker Daltonics). Instrument calibration was performed using a peptide standard kit (Bruker) and, before sample analysis, laser power was adjusted to provide optimal signal-to-noise ratio. For mass fingerprints, brain samples were analyzed with a laser frequency of 1 kHz (3000 laser shots; m/z 600-4000). Ion signals mass-identical with products of the POMC-precursor were selected and fragmented by tandem mass spectrometry (LIFT technology, with acceleration set at 1 kV) using the same samples. Mass spectra obtained in these experiments were processed with the flexAnalysis 3.4 software (Bruker); deduced sequences were counterchecked using the ProteinProspector (http://prospector.ucsf.edu). ClinPro Tools software 3.0 (Bruker) was used for comparison of signal intensities of *Pomc*-products; the results are presented as gel view in logarithmic gray scale display mode.

Electrophysiology

POMC neurons were recorded from NCD/NCD and NCD/HFD POMC^{eGFP} transgenic mice (Cowley et al., 2001) at room temperature under current- and voltage-clamp in the perforated patch and whole-cell patch-clamp configuration using an EPC10 patch-clamp amplifier (HEKA). The animals were anesthetized with halothane (B4388; Sigma-Aldrich) and decapitated. Coronal slices (250 – 300 μm) containing the arcuate nucleus (ARH) were cut with a vibration microtome (HM-650 V; Thermo Scientific) under cold (4°C), carbogenated (95% O_2 and 5% CO_2), glycerol-based modified artificial cerebrospinal fluid (GaCSF; (Ye et al., 2006)), which contained (in mM): 250 Glycerol, 2.5 KCl, 2 $MgCl_2$, 2 $CaCl_2$, 1.2 NaH_2PO_4, 10 HEPES, 21 $NaHCO_3$, and 5 Glucose adjusted to pH 7.2 with NaOH. If not mentioned otherwise, the brain slices were continuously superfused with carbogenated artificial cerebrospinal fluid (aCSF) at a flow rate of ~2 ml·min-1, which contained (in mM): 125 NaCl, 2.5 KCl, 2 $MgCl_2$, 2 $CaCl_2$, 1.2 NaH_2PO_4, 21 $NaHCO_3$, 10 HEPES, and 5 Glucose adjusted to pH 7.2 with NaOH.

Current-clamp recordings in the perforated patch configuration were performed using protocols modified from Horn and Marty (Horn and Marty, 1988), Rae et al. (Rae et al., 1991) and Akaike and Harata (Akaike and Harata, 1994). The recordings were performed with ATP and GTP free pipette solution containing (in mM): 128 K-gluconate, 10 KCl, 10 HEPES, 0.1 EGTA, 2 $MgCl_2$ and adjusted to pH 7.3 with KOH. The patch pipette was tip filled with internal solution and back filled with tetraethylrhodamine-dextran (D3308; Invitrogen, Eugene) and amphotericin B- (~200 $\mu g \cdot ml^{-1}$; A4888; Sigma) or nystatin-containing (~200 $\mu g \cdot ml^{-1}$; N6261; Sigma) internal solution to achieve perforated patch recordings. For the mean firing rate of POMC neurons, the measured frequency was averaged as soon as it was stable for ~5 mins after perforation reached stable series resistances. Cell input resistance and whole-cell conductance were calculated from voltage responses to hyperpolarizing current pulses.

Whole-cell recordings were performed following the methods of Hamill et al. (Hamill et al., 1981). For measurements of postsynaptic currents (PSCs), the patch pipette solution contained (in mM): 140 KCl, 10 HEPES, 0.1 EGTA, 5 $MgCl_2$, 5 K-ATP, 0.3 Na-GTP; adjusted to pH 7.3 with KOH). Cells were voltage clamped at −60 mV and the high intracellular chloride concentration shifted the chloride equilibrium potential to a more depolarized potential, which reversed the polarity of $GABA_A$ receptor mediated currents from outward to inward, and made their detection easier by increasing the driving force on the chloride ions. The contribution of excitatory (EPSCs) and inhibitory PSCs (IPSCs) to the synaptic input was determined in three steps. First, we measured the overall frequency of PSCs. Second, we blocked the glutamatergic EPSCs with 5×10^{-5} D-AP5 and 10^{-5} M CNQX to isolate the IPSCs, which were identified as GABAergic (inhibitory) PSCs by their sensitivity to 10^{-4} M PTX. The EPSC frequency was determined by subtracting the IPSC frequency from the overall frequency. The overall PSC frequency was determined after the recording had stabilized (>10 minutes after break in) for a 2 minutes interval. The IPSC frequency was measured after 10 – 15 minutes D-AP5/CNQX application for a 2 minutes interval. Ratios of IPSCs are relative to overall PSCs.

AgRP and α-MSH immunostaining and analyses

8- and 20-week-old male mice were anesthetized and transcardially perfused with phosphate buffered saline (PBS), pH 7.5, followed by 4 % paraformaldehyde (PFA) in borate buffer, pH 9.5 and post-fixed for 4 h in 20 % sucrose 4 % PFA in borate buffer and transferred to 20 % sucrose in PBS overnight. Brains were frozen, sectioned at 25 μm and processed for immunofluorescence as described previously (Bouret et al., 2004; Bouret et al., 2008; Steculorum and Bouret, 2011). Briefly, sections were incubated in goat anti-AgRP (1:4000; Phoenix Pharmaceuticals) or sheep anti-α-MSH (1:40000, Millipore). Secondary Alexa Fluor 488 goat antirabbit IgG or Alexa Fluor 568 donkey anti-sheep IgG (1:200, Life Technologies™) were used to detect primary antibodies. Sections were mounted in DAPI-containing Vectashield (Vector Laboratories Inc.). Pictures were acquired using a confocal Leica TCS SP-8-X microscope equipped with a 20x objective. Image analysis was performed in a blind manner using ImageJ software (ImageJ1.45s; National Institutes of Health), as described previously (Bouret et al., 2004; Steculorum and Bouret, 2011). Briefly, the integrated density was calculated for each image, a figure that reflects the total number

of pixels in a given region of the image and that is proportional to the total density of labeled fibers in this region. If there were more than one section per animal in the correct region, the average integrated intensity was used to calculate the ratio to the average integrated density of ctrl animals (i.e. NCD/NCD ctrl), which was used for further statistical analyses.

Insulin and vAChT double-immunostaining and analyses

Frozen pancreata from 20-week-old animals were sectioned at 10 μm at three different levels, collected on microscope slides and frozen at −20°C until further use. Microscope slides were warmed up to room temperature (RT) for 20 mins and fixed with 4 % PFA in PBS, pH 7.5 for 10 mins. The slides were then rinsed in PBS and subjected to antigen retrieval. Pancreatic sections were blocked in PBS containing 3% donkey serum and 0.3 % Triton X (Sigma) for 1 h at RT and subsequently incubated in goat anti-vACht (1:100, Millipore) and guinea-pig anti-Insulin (1:500, Dako) in PBS containing 3 % donkey serum and 0.3 % Triton X overnight at RT. Primary antibodies were detected with Alexa Fluor488 donkey anti-goat IgG (1:500, Life Technologies™) and Cy3 donkey anti-guinea-pig (1:500, Jackson ImmunoResearch Laboratories, Inc.) for 1 h at RT. 10-15 islets per animal were acquired using a confocal Leica TCS SP-8-X microscope equipped with a 40x objective. Image analysis was performed using ImageJ software (ImageJ1.45s; National Institutes of Health). Briefly, each vAChT-immunoreactive button that could clearly be distinguished from background signal was counted and set in relation to the insulin-immunoreactive islet size. The average relative number of vAChT-immunoreactive buttons of all islets from one animal was used to calculate its ratio to the average number of the relative vAChT-immunoreactive buttons of control animals (i.e. NCD/NCD ctrl), which was used for further statistical analyses.

Analysis of pancreatic β-cell mass

Pancreatic sections were fixed with acetone for 10 mins at 4°C. Subsequently, sections were first blocked in PBS containing 1 % BSA and 0.3 % H_2O_2 and after washing 3x with PBS, blocked in Rotiblock (1:10 with PBS, Roth®) containing 0.1 % Triton X. Incubation with guinea pig anti-insulin (1:50, DAKO) for 60 mins was followed by 3x washing with PBS and a 60 mins incubation with secondary horse-radish peroxidase (HRP)-coupled anti-guinea-pig (HRP; 1:500, Jackson ImmunoResearch Laboratories, Inc.) in PBS containing 0.25 % Triton X. HRP was detected using liquid diaminobenzidine + chromogene Substrate (1:50, Dako) for 20 mins. Sections were counter-stained with Mayer's Haematoxylin for 3 mins. Pictures were acquired using the LeicaSCN400 slidescanner for brightfield images equipped with a 20x objective (Leica, Germany).

Supplementary Material

Refer to Web version on PubMed Central for supplementary material.

Acknowledgments

References

Anna V, van der Ploeg HP, Cheung NW, Huxley RR, Bauman AE. Sociodemographic Correlates of the Increasing Trend in Prevalence of Gestational Diabetes Mellitus in a Large Population of Women Between 1995 and 2005. Diabetes care. 2008; 31:2288–2293. [PubMed: 18809630]

Balthasar N, Coppari R, McMinn J, Liu SM, Lee CE, Tang V, Kenny CD, McGovern RA, Chua SC Jr. Elmquist JK, et al. Leptin receptor signaling in POMC neurons is required for normal body weight homeostasis. Neuron. 2004; 42:983–991. [PubMed: 15207242]

Baum P, Petroff D, Classen J, Kiess W, Bluher S. Dysfunction of autonomic nervous system in childhood obesity: a cross-sectional study. PloS one. 2013; 8:e54546. [PubMed: 23358101]

Belgardt BF, Bruning JC. CNS leptin and insulin action in the control of energy homeostasis. Annals of the New York Academy of Sciences. 2010; 1212:97–113. [PubMed: 21070248]

Biag J, Huang Y, Gou L, Hintiryan H, Askarinam A, Hahn JD, Toga AW, Dong HW. Cyto- and chemoarchitecture of the hypothalamic paraventricular nucleus in the C57BL/6J male mouse: a study of immunostaining and multiple fluorescent tract tracing. The Journal of comparative neurology. 2012; 520:6–33. [PubMed: 21674499]

Bonnin A, Levitt P. Fetal, maternal, and placental sources of serotonin and new implications for developmental programming of the brain. Neuroscience. 2011; 197:1–7. [PubMed: 22001683]

Bouret SG, Draper SJ, Simerly RB. Formation of projection pathways from the arcuate nucleus of the hypothalamus to hypothalamic regions implicated in the neural control of feeding behavior in mice. The Journal of neuroscience : the official journal of the Society for Neuroscience. 2004a; 24:2797–2805. [PubMed: 15028773]

Bouret SG, Draper SJ, Simerly RB. Trophic action of leptin on hypothalamic neurons that regulate feeding. Science. 2004b; 304:108–110. [PubMed: 15064420]

Bouret SG, Gorski JN, Patterson CM, Chen S, Levin BE, Simerly RB. Hypothalamic neural projections are permanently disrupted in diet-induced obese rats. Cell metabolism. 2008; 7:179–185. [PubMed: 18249177]

Bouyer K, Simerly RB. Neonatal leptin exposure specifies innervation of presympathetic hypothalamic neurons and improves the metabolic status of leptin-deficient mice. The Journal of neuroscience : the official journal of the Society for Neuroscience. 2013; 33:840–851. [PubMed: 23303959]

Broberger C, Hokfelt T. Hypothalamic and vagal neuropeptide circuitries regulating food intake. Physiology & behavior. 2001; 74:669–682. [PubMed: 11790430]

Bruning JC, Michael MD, Winnay JN, Hayashi T, Horsch D, Accili D, Goodyear LJ, Kahn CR. A muscle-specific insulin receptor knockout exhibits features of the metabolic syndrome of NIDDM without altering glucose tolerance. Molecular cell. 1998; 2:559–569. [PubMed: 9844629]

Catalano PM, Presley L, Minium J, Hauguel-de Mouzon S. Fetuses of obese mothers develop insulin resistance in utero. Diabetes care. 2009; 32:1076–1080. [PubMed: 19460915]

Chen H, Simar D, Lambert K, Mercier J, Morris MJ. Maternal and postnatal overnutrition differentially impact appetite regulators and fuel metabolism. Endocrinology. 2008; 149:5348–5356. [PubMed: 18635655]

Clausen TD, Mathiesen ER, Hansen T, Pedersen O, Jensen DM, Lauenborg J, Damm P. High Prevalence of Type 2 Diabetes and Pre-Diabetes in Adult Offspring of Women With Gestational Diabetes Mellitus or Type 1 Diabetes The role of intrauterine hyperglycemia. Diabetes care. 2008; 31:340–346. [PubMed: 18000174]

Cowley MA, Smart JL, Rubinstein M, Cerdan MG, Diano S, Horvath TL, Cone RD, Low MJ. Leptin activates anorexigenic POMC neurons through a neural network in the arcuate nucleus. Nature. 2001; 411:480–484. [PubMed: 11373681]

Creemers JW, Pritchard LE, Gyte A, Le Rouzic P, Meulemans S, Wardlaw SL, Zhu X, Steiner DF, Davies N, Armstrong D, et al. Agouti-related protein is posttranslationally cleaved by proprotein convertase 1 to generate agouti-related protein (AGRP)83-132: interaction between AGRP83-132

and melanocortin receptors cannot be influenced by syndecan-3. Endocrinology. 2006; 147:1621–1631. [PubMed: 16384863]

Deierlein AL, Siega-Riz AM, Chantala K, Herring AH. The Association Between Maternal Glucose Concentration and Child BMI at Age 3 Years. Diabetes care. 2011; 34:480–484. [PubMed: 21216858]

Fekete C, Kelly J, Mihaly E, Sarkar S, Rand WM, Legradi G, Emerson CH, Lechan RM. Neuropeptide Y has a central inhibitory action on the hypothalamic-pituitary-thyroid axis. Endocrinology. 2001; 142:2606–2613. [PubMed: 11356711]

Fekete C, Legradi G, Mihaly E, Huang QH, Tatro JB, Rand WM, Emerson CH, Lechan RM. alpha-Melanocyte-stimulating hormone is contained in nerve terminals innervating thyrotropin-releasing hormone-synthesizing neurons in the hypothalamic paraventricular nucleus and prevents fasting-induced suppression of prothyrotropin-releasing hormone gene expression. The Journal of neuroscience : the official journal of the Society for Neuroscience. 2000; 20:1550–1558. [PubMed: 10662844]

Franklin, KBJ.; Paxinos, G. The Mouse Brain in Stereotactic Coordinates. Academic Press; 1997.

Glavas MM, Kirigiti MA, Xiao XQ, Enriori PJ, Fisher SK, Evans AE, Grayson BE, Cowley MA, Smith MS, Grove KL. Early overnutrition results in early-onset arcuate leptin resistance and increased sensitivity to high-fat diet. Endocrinology. 2010; 151:1598–1610. [PubMed: 20194730]

Gorski JN, Dunn-Meynell AA, Hartman TG, Levin BE. Postnatal environment overrides genetic and prenatal factors influencing offspring obesity and insulin resistance. American journal of physiology Regulatory, integrative and comparative physiology. 2006; 291:R768–778.

Grant WF, Nicol LE, Thorn SR, Grove KL, Friedman JE, Marks DL. Perinatal exposure to a high-fat diet is associated with reduced hepatic sympathetic innervation in one-year old male Japanese macaques. PloS one. 2012; 7:e48119. [PubMed: 23118937]

Gravena C, Andreazzi AE, Mecabo FT, Grassiolli S, Scantamburlo VM, Mathias PC. Protein restriction during lactation alters the autonomic nervous system control on glucose-induced insulin secretion in adult rats. Nutritional neuroscience. 2007; 10:79–87. [PubMed: 17539486]

Grayson BE, Allen SE, Billes SK, Williams SM, Smith MS, Grove KL. Prenatal development of hypothalamic neuropeptide systems in the nonhuman primate. Neuroscience. 2006; 143:975–986. [PubMed: 17029798]

Greenfield JR, Campbell LV. Role of the autonomic nervous system and neuropeptides in the development of obesity in humans: targets for therapy? Current pharmaceutical design. 2008; 14:1815–1820. [PubMed: 18673184]

Gropp E, Shanabrough M, Borok E, Xu AW, Janoschek R, Buch T, Plum L, Balthasar N, Hampel B, Waisman A, et al. Agouti-related peptide-expressing neurons are mandatory for feeding. Nature neuroscience. 2005; 8:1289–1291.

Grove KL, Cowley MA. Is ghrelin a signal for the development of metabolic systems? The Journal of clinical investigation. 2005; 115:3393–3397. [PubMed: 16322785]

Grove KL, Grayson BE, Glavas MM, Xiao XQ, Smith MS. Development of metabolic systems. Physiology & behavior. 2005; 86:646–660. [PubMed: 16289141]

Gupta A, Srinivasan M, Thamadilok S, Patel MS. Hypothalamic alterations in fetuses of high fat diet-fed obese female rats. The Journal of endocrinology. 2009; 200:293–300. [PubMed: 19074472]

Habbout A, Li N, Rochette L, Vergely C. Postnatal overfeeding in rodents by litter size reduction induces major short- and long-term pathophysiological consequences. The Journal of nutrition. 2013; 143:553–562. [PubMed: 23446961]

Harder T, Rake A, Rohde W, Doerner G, Plagemann A. Overweight and increased diabetes susceptibility in neonatally insulin-treated adult rats. Endocrine regulations. 1999; 33:25–31. [PubMed: 10200585]

Horvath TL, Bruning JC. Developmental programming of the hypothalamus: a matter of fat. Nature medicine. 2006; 12:52–53. discussion 53.

Kim SY, England JL, Sharma JA, Njoroge T. Gestational diabetes mellitus and risk of childhood overweight and obesity in offspring: a systematic review. Experimental diabetes research. 2011; 2011:541308. [PubMed: 21960991]

King CM, Hentges ST. Relative number and distribution of murine hypothalamic proopiomelanocortin neurons innervating distinct target sites. PloS one. 2011; 6:e25864. [PubMed: 21991375]

Klockener T, Hess S, Belgardt BF, Paeger L, Verhagen LA, Husch A, Sohn JW, Hampel B, Dhillon H, Zigman JM, et al. High-fat feeding promotes obesity via insulin receptor/PI3K-dependent inhibition of SF-1 VMH neurons. Nature neuroscience. 2011; 14:911–918.

Konner AC, Janoschek R, Plum L, Jordan SD, Rother E, Ma X, Xu C, Enriori P, Hampel B, Barsh GS, et al. Insulin action in AgRP-expressing neurons is required for suppression of hepatic glucose production. Cell metabolism. 2007; 5:438–449. [PubMed: 17550779]

Konner AC, Klockener T, Bruning JC. Control of energy homeostasis by insulin and leptin: targeting the arcuate nucleus and beyond. Physiology & behavior. 2009; 97:632–638. [PubMed: 19351541]

Koutcherov Y, Mai JK, Paxinos G. Hypothalamus of the human fetus. Journal of chemical neuroanatomy. 2003; 26:253–270. [PubMed: 14729128]

Ludwig DS, Ebbeling CB. Type 2 diabetes mellitus in children: primary care and public health considerations. JAMA : the journal of the American Medical Association. 2001; 286:1427–1430. [PubMed: 11572718]

Luquet S, Perez FA, Hnasko TS, Palmiter RD. NPY/AgRP neurons are essential for feeding in adult mice but can be ablated in neonates. Science. 2005; 310:683–685. [PubMed: 16254186]

Marino JS, Xu Y, Hill JW. Central insulin and leptin-mediated autonomic control of glucose homeostasis. Trends in endocrinology and metabolism: TEM. 2011; 22:275–285. [PubMed: 21489811]

Metzger BE, Lowe LP, Dyer AR, Trimble ER, Chaovarindr U, Coustan DR, Hadden DR, McCance DR, Hod M, McIntyre HD, et al. Hyperglycemia and adverse pregnancy outcomes. The New England journal of medicine. 2008; 358:1991–2002. [PubMed: 18463375]

Morris MJ, Chen H. Established maternal obesity in the rat reprograms hypothalamic appetite regulators and leptin signaling at birth. Int J Obes (Lond). 2009; 33:115–122. [PubMed: 18982008]

Mumtaz M. Gestational diabetes mellitus. The Malaysian journal of medical sciences : MJMS. 2000; 7:4–9. [PubMed: 22844208]

Pedersen J. Diabetes mellitus and pregnancy: present status of the hyperglycaemia--hyperinsulinism theory and the weight of the newborn baby. Postgraduate medical journal. 1971; (Suppl):66–67. [PubMed: 5547509]

Plagemann, A. Perinatal programming : the state of the art. De Gruyter; Berlin ; Boston: 2012.

Plagemann A, Harder T, Janert U, Rake A, Rittel F, Rohde W, Dorner G. Malformations of hypothalamic nuclei in hyperinsulinemic offspring of rats with gestational diabetes. Developmental neuroscience. 1999; 21:58–67. [PubMed: 10077703]

Plagemann A, Heidrich I, Gotz F, Rohde W, Dorner G. Lifelong enhanced diabetes susceptibility and obesity after temporary intrahypothalamic hyperinsulinism during brain organization. Experimental and clinical endocrinology. 1992; 99:91–95. [PubMed: 1639125]

Pritchard LE, White A. Neuropeptide processing and its impact on melanocortin pathways. Endocrinology. 2007; 148:4201–4207. [PubMed: 17584964]

Rossi J, Balthasar N, Olson D, Scott M, Berglund E, Lee CE, Choi MJ, Lauzon D, Lowell BB, Elmquist JK. Melanocortin-4 receptors expressed by cholinergic neurons regulate energy balance and glucose homeostasis. Cell metabolism. 2011; 13:195–204. [PubMed: 21284986]

Rossi J, Santamaki P, Airaksinen MS, Herzig KH. Parasympathetic innervation and function of endocrine pancreas requires the glial cell line-derived factor family receptor alpha2 (GFRalpha2). Diabetes. 2005; 54:1324–1330. [PubMed: 15855316]

Sabin MA, Shield JP. Childhood obesity. Frontiers of hormone research. 2008; 36:85–96. [PubMed: 18230896]

Sasaki A, de Vega WC, St-Cyr S, Pan P, McGowan PO. Perinatal high fat diet alters glucocorticoid signaling and anxiety behavior in adulthood. Neuroscience. 2013; 240:1–12. [PubMed: 23454542]

Schechter R, Abboud M, Johnson G. Brain endogenous insulin effects on neurite growth within fetal rat neuron cell cultures. Brain research Developmental brain research. 1999; 116:159–167. [PubMed: 10521560]

Segerson TP, Hoefler H, Childers H, Wolfe HJ, Wu P, Jackson IM, Lechan RM. Localization of thyrotropin-releasing hormone prohormone messenger ribonucleic acid in rat brain in situ hybridization. Endocrinology. 1987; 121:98–107. [PubMed: 3109882]

Sohn JW, Harris LE, Berglund ED, Liu T, Vong L, Lowell BB, Balthasar N, Williams KW, Elmquist JK. Melanocortin 4 receptors reciprocally regulate sympathetic and parasympathetic preganglionic neurons. Cell. 2013; 152:612–619. [PubMed: 23374353]

Steculorum SM, Bouret SG. Maternal diabetes compromises the organization of hypothalamic feeding circuits and impairs leptin sensitivity in offspring. Endocrinology. 2011; 152:4171–4179. [PubMed: 21862611]

Steculorum SM, Vogt MC, Bruning JC. Perinatal programming of metabolic diseases: role of insulin in the development of hypothalamic neurocircuits. Endocrinology and metabolism clinics of North America. 2013; 42:149–164. [PubMed: 23391245]

Sullivan EL, Grove KL. Metabolic imprinting in obesity. Forum of nutrition. 2010; 63:186–194. [PubMed: 19955786]

Sun B, Purcell RH, Terrillion CE, Yan J, Moran TH, Tamashiro KL. Maternal high-fat diet during gestation or suckling differentially affects offspring leptin sensitivity and obesity. Diabetes. 2012; 61:2833–2841. [PubMed: 22751689]

Swanson, LW. Brain Maps: Structure of the Rat Brain. Academic Press; 1998.

Toran-Allerand CD, Ellis L, Pfenninger KH. Estrogen and insulin synergism in neurite growth enhancement in vitro: mediation of steroid effects by interactions with growth factors? Brain research. 1988; 469:87–100. [PubMed: 3042097]

Vickers MH, Gluckman PD, Coveny AH, Hofman PL, Cutfield WS, Gertler A, Breier BH, Harris M. Neonatal leptin treatment reverses developmental programming. Endocrinology. 2005; 146:4211–4216. [PubMed: 16020474]

Vogt MC, Bruning JC. CNS insulin signaling in the control of energy homeostasis and glucose metabolism - from embryo to old age. Trends in endocrinology and metabolism: TEM. 2013; 24:76–84. [PubMed: 23265947]

Williams KW, Margatho LO, Lee CE, Choi M, Lee S, Scott MM, Elias CF, Elmquist JK. Segregation of acute leptin and insulin effects in distinct populations of arcuate proopiomelanocortin neurons. The Journal of neuroscience : the official journal of the Society for Neuroscience. 2010; 30:2472–2479. [PubMed: 20164331]

Yu Z, Han S, Zhu J, Sun X, Ji C, Guo X. Pre-pregnancy body mass index in relation to infant birth weight and offspring overweight/obesity: a systematic review and meta-analysis. PloS one. 2013; 8:e61627. [PubMed: 23613888]

Akaike N, Harata N. Nystatin perforated patch recording and its applications to analyses of intracellular mechanisms. The Japanese journal of physiology. 1994; 44:433–473. [PubMed: 7534361]

Bouret SG, Draper SJ, Simerly RB. Trophic action of leptin on hypothalamic neurons that regulate feeding. Science. 2004; 304:108–110. [PubMed: 15064420]

Bouret SG, Gorski JN, Patterson CM, Chen S, Levin BE, Simerly RB. Hypothalamic neural projections are permanently disrupted in diet-induced obese rats. Cell metabolism. 2008; 7:179–185. [PubMed: 18249177]

Cowley MA, Smart JL, Rubinstein M, Cerdan MG, Diano S, Horvath TL, Cone RD, Low MJ. Leptin activates anorexigenic POMC neurons through a neural network in the arcuate nucleus. Nature. 2001; 411:480–484. [PubMed: 11373681]

Hamill OP, Marty A, Neher E, Sakmann B, Sigworth FJ. Improved patch-clamp techniques for high-resolution current recording from cells and cell-free membrane patches. Pflugers Archiv : European journal of physiology. 1981; 391:85–100. [PubMed: 6270629]

Horn R, Marty A. Muscarinic activation of ionic currents measured by a new whole-cell recording method. The Journal of general physiology. 1988; 92:145–159. [PubMed: 2459299]

Konner AC, Janoschek R, Plum L, Jordan SD, Rother E, Ma X, Xu C, Enriori P, Hampel B, Barsh GS, et al. Insulin action in AgRP-expressing neurons is required for suppression of hepatic glucose production. Cell metabolism. 2007; 5:438–449. [PubMed: 17550779]

Matthews DR, Hosker JP, Rudenski AS, Naylor BA, Treacher DF, Turner RC. Homeostasis model assessment: insulin resistance and beta-cell function from fasting plasma glucose and insulin concentrations in man. Diabetologia. 1985; 28:412–419. [PubMed: 3899825]

Rae J, Cooper K, Gates P, Watsky M. Low access resistance perforated patch recordings using amphotericin B. Journal of neuroscience methods. 1991; 37:15–26. [PubMed: 2072734]

Rappsilber J, Mann M, Ishihama Y. Protocol for micro-purification, enrichment, pre-fractionation and storage of peptides for proteomics using StageTips. Nature protocols. 2007; 2:1896–1906.

Steculorum SM, Bouret SG. Maternal diabetes compromises the organization of hypothalamic feeding circuits and impairs leptin sensitivity in offspring. Endocrinology. 2011; 152:4171–4179. [PubMed: 21862611]

Tong Q, Ye CP, Jones JE, Elmquist JK, Lowell BB. Synaptic release of GABA by AgRP neurons is required for normal regulation of energy balance. Nature neuroscience. 2008; 11:998–1000.

Ye JH, Zhang J, Xiao C, Kong JQ. Patch-clamp studies in the CNS illustrate a simple new method for obtaining viable neurons in rat brain slices: glycerol replacement of NaCl protects CNS neurons. Journal of neuroscience methods. 2006; 158:251–259. [PubMed: 16842860]

Highlights

- Maternal HFD-feeding during lactation impairs metabolic health of the offspring

- Maternal HFD during lactation impairs formation of melanocortin projections

- Abnormal insulin action in POMC-neurons impairs POMC projections to preautonomic PVH

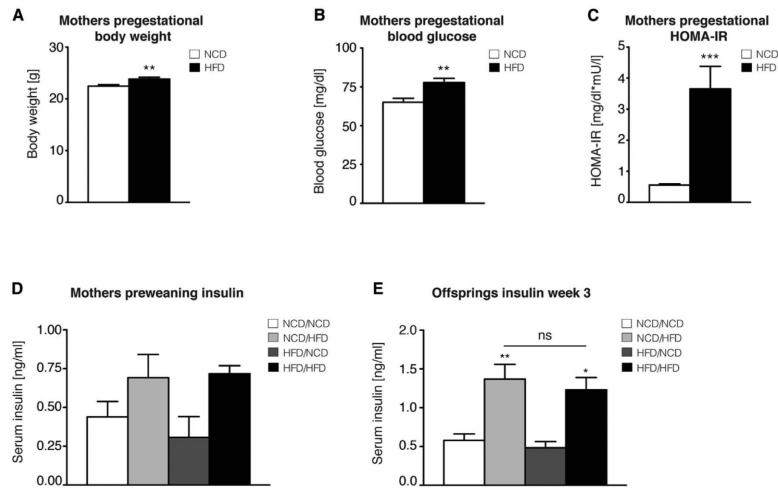- Abrogating POMC insulin action improves glucose metabolism despite maternal HFD

Figure 1. Maternal HFD-feeding induces pregestational metabolic abnormalities and hyperinsulinemia during lactation in the offspring

Maternal (A) pregestational body weight, (B) fasted blood glucose levels and (C) homeostatic model assessment indices of insulin resistance (HOMA-IR) (n=48*vs*50). (D) Maternal preweaning serum insulin levels in the fed state (n=4 for all groups). (E) Serum insulin levels in the offspring at 3 weeks of age (n=9 for all groups). NCD=normal chow diet, HFD=high fat diet. Data are presented as mean ± SEM, **p < 0.01, ***p < 0.001 versus all other groups within the same diet after week 8, if not indicated otherwise. See also Figure S1 for an overview of all experimental groups.
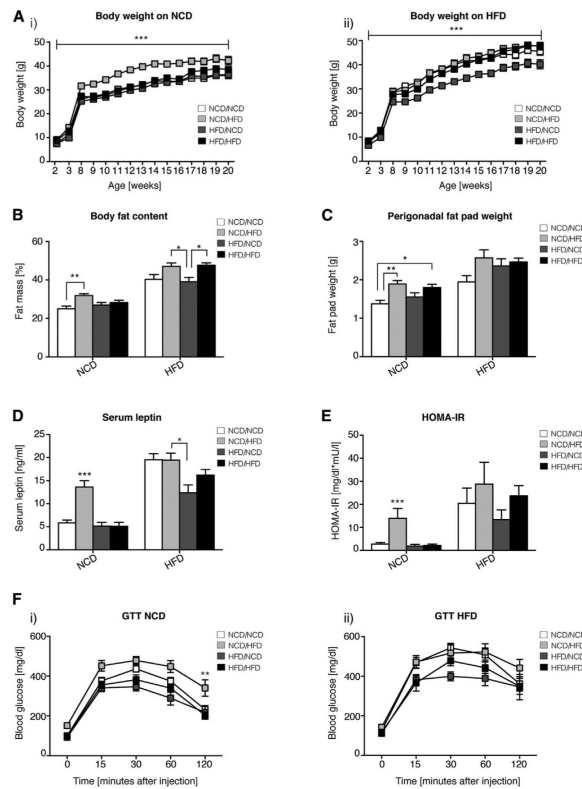
Figure 2. Maternal HFD-feeding exclusively during lactation predisposes the offspring for metabolic disorders

The following metabolic parameters were analyzed in all eight groups of male offspring. (A) Body weight on (i) normal chow diet (NCD; n=14*vs*10*vs*14*vs*13) or (ii) high fat diet (HFD; n=10*vs*8*vs*13*vs*12), (B) body fat content and (C) perigonadal fat pad weight at 20 weeks (n_{NCD}=14*vs*10*vs*13*vs*12 and n_{HFD}=10*vs*8*vs*12*vs*11), (D) fasted serum leptin levels and (E) homeostatic model assessment indices of insulin resistance (HOMA-IR) at 15 weeks (n_{NCD}=13*vs*8*vs*11*vs*9 and n_{HFD}=9*vs*8*vs*11*vs*11) and (F) glucose tolerance tests (GTT) at 15 weeks of age on i) NCD (n=13*vs*10*vs*14*vs*13) and ii) HFD (n=10*vs*8*vs*9*vs*12). Data are presented as mean ± SEM, *p < 0.05. **p < 0.01. ***p < 0.001 versus all other groups within the same diet after 8 weeks of age, unless otherwise indicated. See also Figure S2 for data on female offspring.
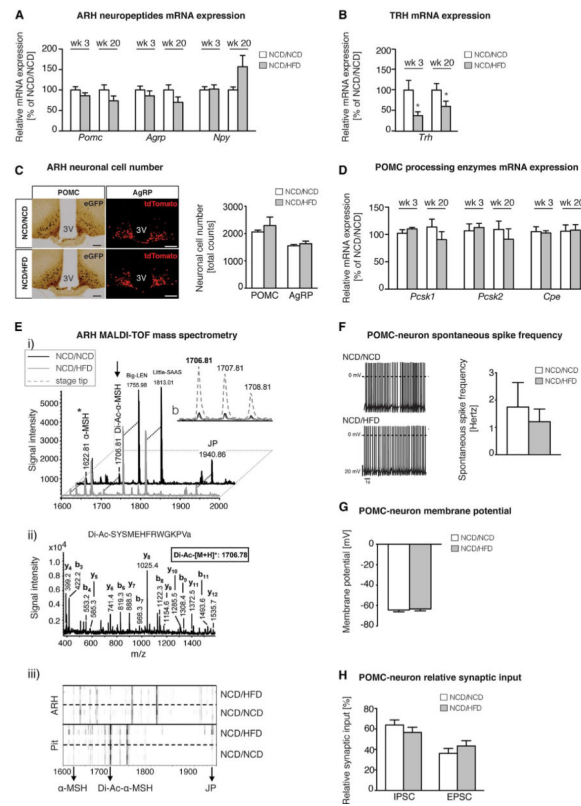
Figure 3. Effects of maternal HFD-feeding during lactation on hypothalamic neurocircuits
All following analyses were performed in NCD/NCD and NCD/HFD male offspring.
Quantitative real-time PCR analysis of hypothalamic (A) *pro-opiomelanocortin* (*Pomc*),
agouti-related peptide (*Agrp*) and *neuropeptide Y* (*Npy*) and (B) *thyrotropin-releasing
hormone* (*Trh*) mRNA expression at 3 (n=9*vs*11) and 20 weeks (n=8*vs*9) of age on NCD.
(C) Analysis of POMC (left) and AgRP (right) neurons in the arcuate nucleus of the
hypothalamus (ARH) in POMC^eGFP and AgRP^tdTomato mice, respectively, at 8 weeks of age
(n_POMC=3*vs*3 and n_AgRP=4*vs*5; scale bar = 100 μm). (D) Quantitative real-time PCR
analysis of hypothalamic *proprotein convertase subtilisin/kexin type 1* (*Pcsk1*), *proprotein
convertase subtilisin/kexin type 2* (*Pcsk2*) and *carboxypeptidase E* (*Cpe*) mRNA expression
at 3 (n=9*vs*11) and 20 weeks (n=8*vs*9) of age on NCD. (E) MALDITOF mass spectra
obtained by profiling extracts of the ARH at 20 weeks of age (n=4*vs*4). Prominent ion
signals are labeled. i) Comparison of mass fingerprints showing nearly identical ion signals,
including ions that are mass-identical with products of the POMC precursor (α-MSH, Di-
Ac-MSH, joining peptide (JP)). Fragmentation experiments confirmed the sequences of all
labeled peptides; the ion-signal at 1622.81 (asterisk) is composed of two substances
(including α-MSH). The arrow marks processed and biologically more potent di-acetylated
α-MSH. b) Isotopic pattern and signal intensity of di-acetylated α-MSH before (lower
traces) and after Stage Tip concentration. ii) MALDI-TOF/TOF fragment spectrum of di-
acetylated α-MSH purified and concentrated with Stage Tips. Y- and b-type fragment ions
are labelled, which confirmed the amino acid sequence of di-acetylated α-MSH. iii) Gel
view of mass spectra (n=4 each) from preparation of ARH and pituitary gland (Pit)
demonstrating identical processing of *Pomc*-products in all samples. (F) Spontaneous spike

frequency and (G) membrane potential of POMC^{eGFP} neurons obtained by perforated patch clamp recordings (n=13 neurons obtained from n=3 animals for each group). (H) Whole-cell recordings showing the relative synaptic input on POMC^{eGFP} neurons (n=13vs14 neurons obtained from n=5vs8 mice). Data are presented as mean ± SEM, *p < 0.05 versus all other groups at the same age. See also Figure S3 for hypothalamic mRNA expression of inflammatory markers at 3 and 20 weeks of age.
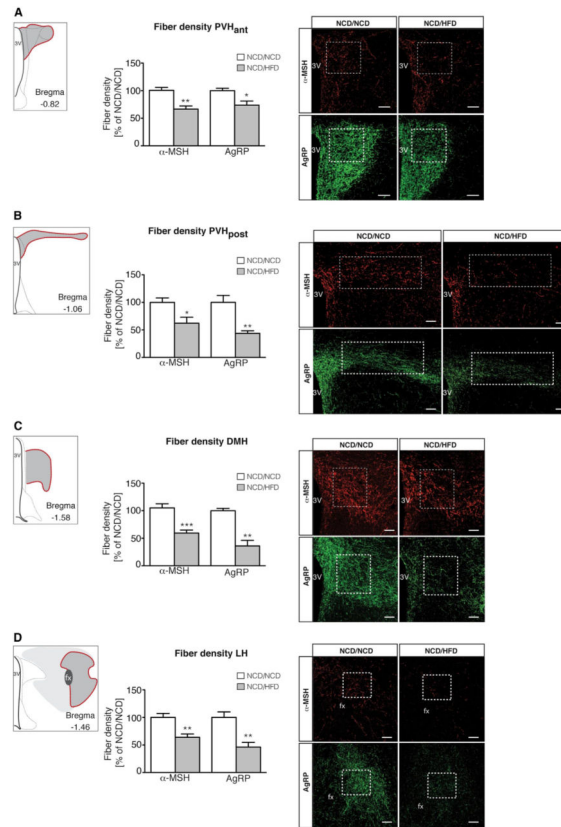
Figure 4. Maternal HFD-feeding exclusively during lactation impairs axonal projections of ARH neurons to intrahypothalamic target sites

Images and quantification of α-melanocyte-stimulating hormone (α-MSH) and agouti-related peptide (AgRP) immunoreactive fibers innervating (A) the anterior endocrine paraventricular nucleus of the hypothalamus (PVH$_{ant}$; n$_{α-MSH}$ =6vs7 and n$_{AgRP}$=7vs7), (B) the posterior preautonomic PVH$_{post}$ (n$_{α-MSH}$ =5vs5 and n$_{AgRP}$=4vs4), (C) the dorsomedial nucleus of the hypothalamus (DMH; n$_{α-MSH}$ =7vs7 and n$_{AgRP}$=4vs5) and (D) the lateral hypothalamic area (LH; n$_{α-MSH}$ =6vs6 and n$_{AgRP}$=6vs4) at 8 weeks of age. Schematics illustrating the localization in the CNS of the respective hypothalamic nuclei presented in the pictures were based on and modified from Brain Maps: Structure of the Rat Brain (Swanson, 1998). Coordinates were adapted according to the Mouse Brain in Stereotaxic Coordinates (Franklin and Paxinos, 1997). White boxes indicate area of quantification. 3V = third ventricle, fx = fornix. Scale bar = 100 μm. Data are presented as mean ± SEM, *p < 0.05. **p < 0.01 versus all other groups of offspring.
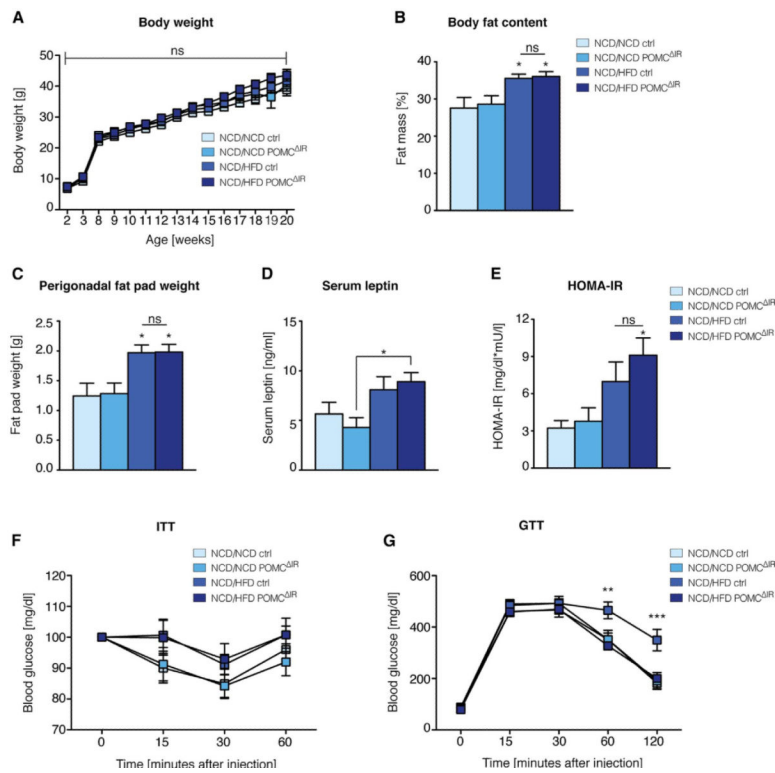
Figure 5. POMC-specific IR-deficiency does not protect from adiposity or insulin resistance, but improves glucose tolerance in NCD/HFD offspring

(A) Body weight (n=10*vs*13*vs*14*vs*14), (B) body fat content (n=9*vs*12*vs*14*vs*14) and (C) perigonadal fat pad weight (n=10*vs*12*vs*14*vs*14) at 20 weeks of age. (D) Fasted serum leptin levels (n=9*vs*9*vs*9*vs*14) and (E) homeostatic model assessment indices of insulin resistance (HOMA-IR; n=6*vs*10*vs*10*vs*14)) at 15 weeks, (F) insulin tolerance tests (ITT) at 14 weeks (n=16*vs*19*vs*20*vs*19) and glucose tolerance tests (GTT) at 15 weeks of age (n=10*vs*13*vs*13*vs*14). Data are presented as mean ± SEM, *p < 0.05. **p < 0.01. ***p < 0.001 versus all other groups of offspring, unless otherwise indicated. See also Figure S4 for data on milk composition.
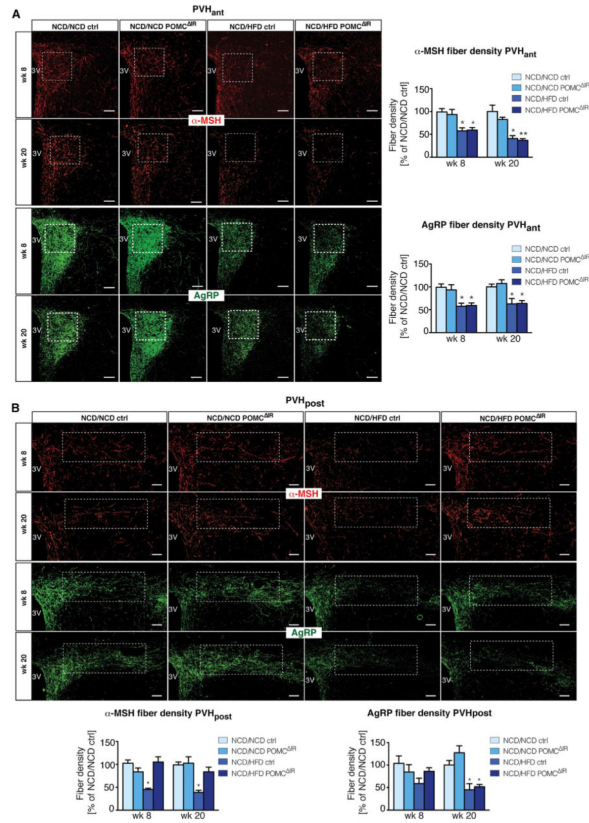
Figure 6. POMC-specific IR-deficiency in NCD/HFD offspring rescues POMC axonal projections to preautonomic regions in the PVH

Images and quantification of α-melanocyte-stimulating hormone (α-MSH) and agouti-related-peptide (AgRP) immunoreactive fibers innervating (A) the anterior neuroendocrine paraventricular nucleus of the hypothalamus (PVH$_{ant}$) at 8 (n$_{\alpha\text{-MSH}}$ and n$_{AgRP}$ =8vs8vs8vs10) and 20 weeks of age (n = 5 for all groups); and (B) the posterior preautonomic PVH (PVH$_{post}$) at 8 (n$_{\alpha\text{-MSH}}$ =7vs6vs5vs6 and n$_{AgRP}$=5vs6vs5vs6) and 20 weeks of age (n= 5 for all groups). White boxes indicate area of quantification. 3V= third ventricle. Scale bar = 100 μm. Data are presented as mean ± SEM, *p < 0.05 versus all other groups of offspring, unless otherwise indicated. See also S5 for images and quantification of α-MSH and AgRP immunoreactive fibers innervating the dorsomedial nucleus of the hypothalamus (DMH) and the lateral hypothalamic area (LH) at 20 weeks of age.
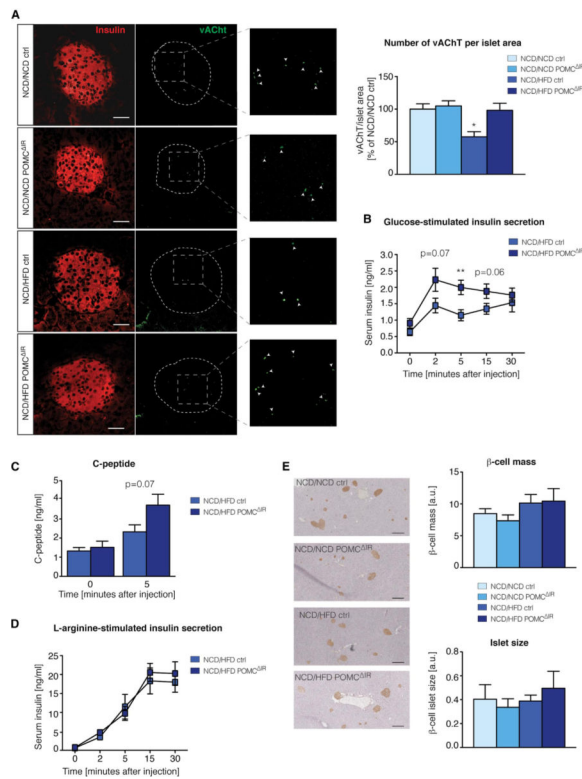
Figure 7. Effects of maternal HFD-feeding during lactation and POMC-specific IR-deficiency on pancreatic β-cells

(A) Images and quantification of the parasympathetic marker vesicular acetylcholine transporter (vAChT, green) on pancreatic β-cells (insulin, red) at 20 weeks of age (n=6*vs*5*vs*8*vs*6). Scale bar = 50 μm. (B) Glucose-stimulated insulin secretion (n=13*vs*13), (C) C-peptide levels 0 and 5 minutes after glucose injection (n=8*vs*8) (See also S6 for corresponding glucagon-like peptide 1 and free fatty acid concentrations), and (D) L-arginine-stimulated insulin secretion at 15 weeks of age (n=7*vs*7). (E) Images and quantification of total β-cell mass and average β-cell islet size at 20 weeks of age (n=6*vs*5*vs*4*vs*5). Scale bar = 300 μm. Data are presented as mean ± SEM, *p < 0.05 versus all other groups of offspring, unless otherwise indicated.